1. Introduction

If a metal is put it into an oxidizing atmosphere at elevated temperature, oxidation of the metal takes place by either outward diffusion of metal or inward diffusion of oxygen, through the oxide scale.[1] The outward diffusion of metal normally results in the formation of an external scale that grows at the scale-gas interface, as well as the formation of voids and cavities at the scale/alloy interface that can lead to scale spallation. In many cases, it is the properties of this external scale that determine the oxidation resistance of the alloy.[2]

In an earlier paper, inhomogeneity in scale formation at the very early stage of oxidation was observed, that scale ridges can be seen all over the sample surface.[3] The post experiment characterization of the abovementioned observation can be seen in Figure 1. Ridges can be found all over the surface as shown in Figure 1a and details of ridges (indicated by black dotted line) can be seen in Figure 1b. In the cross-section view of a ridge, it is suspected that the ridge grew right on top of an alloy grain boundary.

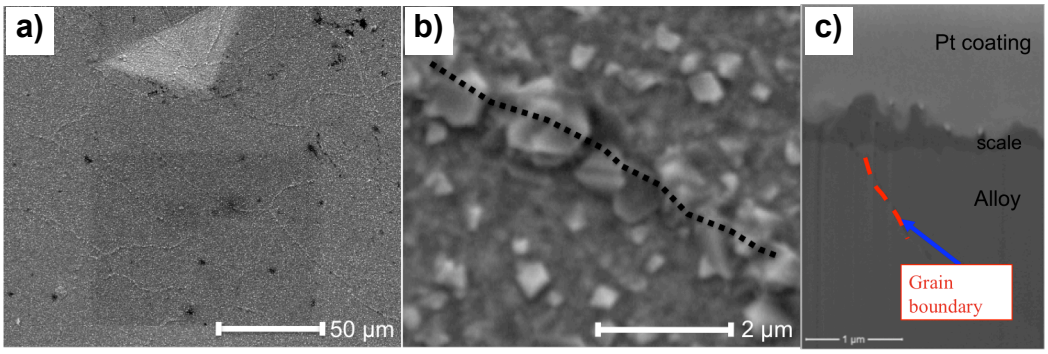

Figure 1 SEM secondary electron images of an Fe-22Cr-0.04RE (F_2) alloy after 15 min oxidation at 800 °C in dry air. a) General view of the surface after oxidation. b) Higher magnification of the ridge formed. c) Cross-section view of the scale ridge.

To confirm the possible relationship between ridges and grain boundaries of the alloy, a random area of scale was reconstructed with serial cross-sectional SEM images of the sample obtained through serial step-wise sectioning using FIB. The reconstructed scale layer is shown in Figure 2. A triple junction of ridges can be seen on the scale layer. The reconstruction shows that the scale layer is made up of oxide nodules (as the one circled in Figure 2), but only those places where the alloy grain boundaries intersect the scale seem to have continuous ridges. The nodule, indicated by the red circle, would appear as a ridge in a 2D cross-section such as those in Figure 1, but it can be seen in the 3D reconstruction that it does not have a grain boundary associated with it in the underlying alloy, and it is clearly not part of a continuous ridge.

The fact that the scale ridge formation was shown to relate to the alloy grain boundaries beneath suggests it to be an fast path diffusion phenomenon. Grain boundary diffusion is a typical type of fast path diffusion.

The purpose of the present investigation is to examine the relationships between fast-path diffusion during transient oxidation with respect to the geometry of alloy grain boundaries by analyzing the scale ridge features and the underlying alloy grain boundary characteristics. The

alloys considered in this study were similar to a Crofer 22 alloy with 22 wt% Cr, in which Ce was also added along with La.

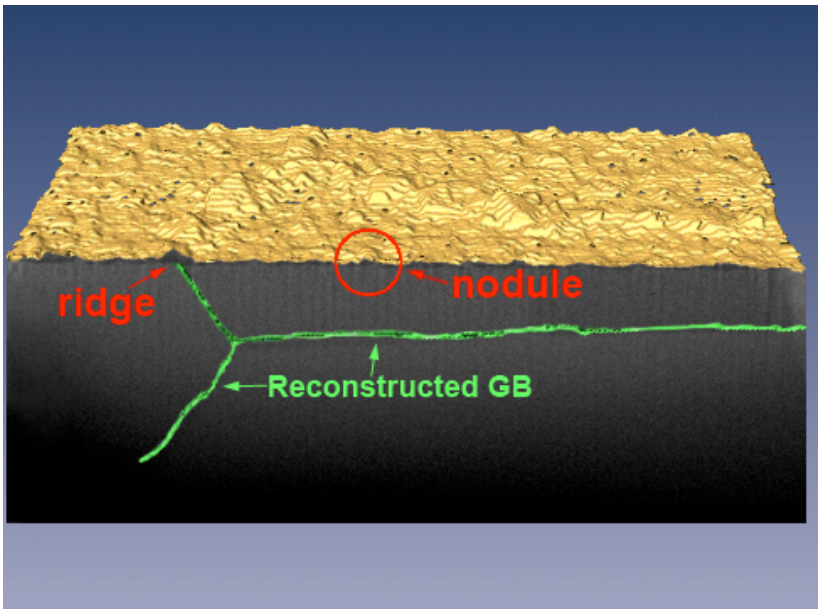

Figure 2 Reconstructed scale layer combined with the SEM image of the cross-section.

2. Experimental

2.1 Alloy Studied

A Fe-22wt%Cr ferritic stainless steel was selected as the base material. Vacuum induction melting was used to produce 7 kg ingots from high purity starting elemental materials. After casting, the alloys were reduced to sheet by hot working and cold rolling. The nominal composition of the alloy was Fe-22Cr-0.04RE.

Samples for the oxidation study were made with dimensions of 4 mm × 4 mm × 1 mm and ground with SiC paper through 1200 grit, and then fine polished with 6, 3 and 1 µm diamond suspensions. These polished samples were subsequently cleaned with soapy water, and then cleaned ultrasonically in acetone and ethanol.

2.2 High Temperature Oxidation and Characterization

The flowchart in Figure 3 shows the several steps performed in the orientation imaging and observation of scale ridge size.

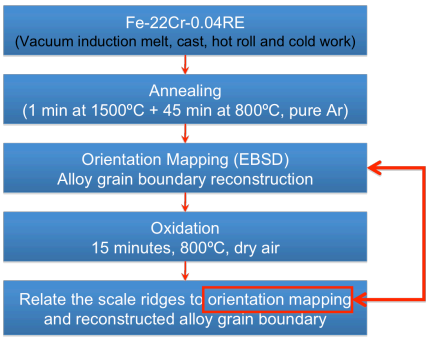

Figure 3 Flowchart of the investigation of the relationship between scale ridge size and alloy grain boundary.

2.2.1 Annealing of the alloy

Since the alloys used in this study were ferritic alloys that lack an allotropic phase transformation, a requirement to ensure that grain boundary migration and growth did not occur during the oxidation experiments existed. To stabilize the alloy grain boundaries and release residual strain from cold work, the specimen was annealed before orientation mapping, for 1 minute at 1500ºC followed by 45 minutes at 800 ºC. The grain structures of the alloy annealed for different conditions were shown in Figure 4. It is clear that the grain structure shown in Figure 4a is not suitable for characterizing grain boundaries. From Figure 4b, texture can still be seen although the sample is recrystalized. It can be seen from Figure 4c that the alloy grains have completely recrystallized and clearly proceeded to the stage of grain coarsening after annealing. No obvious cold worked texture remained. More than 86% of the total length of the grain boundaries was large angle (>15º) boundaries. The grain boundaries seemed quite stable judging from dihedral angles at triple junctions and also the GB curvature, and therefore suitable for the investigation of grain boundary diffusion.[4]

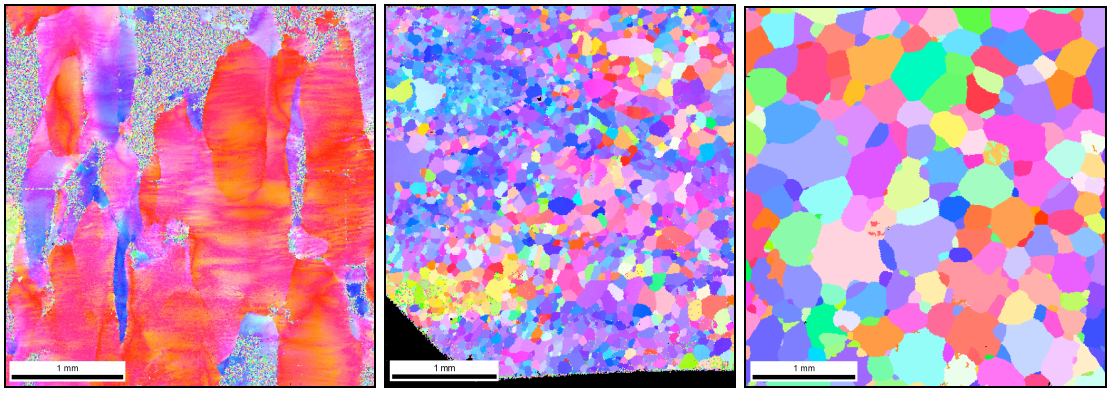

a) **b)** **c)**

Figure 4 EBSD maps of the alloy a) after cold work; b) annealed for 45 minutes at 800ºC in pure Ar; and c) annealed for 1 minute at 1500ºC followed by 45 minutes at 800 ºC in pure Ar.

Another reason that large grains are suitable for the purpose of the current study concerns the kinetics of the grain boundary diffusion since grain size is an important criterion in determining the kinetic regime of such diffusion. Fast path diffusion through grain boundaries can be categorized into three kinetic types; A, B and C, after Harrison.[5] For type A, the material acts as a uniform medium for diffusion with an effective diffusion coefficient; type C represents situations in which diffusion occurs exclusively through the grain boundary (GB), and any case between the two extremes is type B, in which volume diffusion and GB diffusion occur simultaneously. In order to study the grain boundary diffusion with respect to the grain boundary characteristics, type A diffusion must not be in operation, since the overlapping diffusion field, due to a fine grain structure, diminishes the effect on the GB diffusion from individual grain boundary. The quantitative criteria that distinguish the three types of GB diffusion are analyzed by I. Kaur et. al.[6] as follows:

Type A, $(Dt)^{1/2} \geq 150d$;

Type B, $100\delta < (Dt)^{1/2} < d/20$; in some experimental conditions the type B criterion is considered as $10\delta < (Dt)^{1/2} < d/10$, which is less strict;

Type C, $20(Dt)^{1/2} < \delta$;

where D is the volume diffusion coefficient, t the annealing time, d the grain size and δ the grain boundary thickness. The term $(Dt)^{1/2}$ is known as mean diffusion distance.

Plugging in the experimental conditions of the present study, the kinetic regime is determined as follows. The diffusion coefficients of the major alloy elements of the study material can be found in Table 1.

Table 1 Pertinent diffusion coefficient data for substitutional elements.

Alloy	Element	Temperature (K)	E(kJ•mol^{-1})	D_o (cm^2•s^{-1})	Ref.
Fe(BCC)	Fe	1043-1809	240	2.0	[7]
Fe(BCC)	Cr	1048-1971	238.8	2.33	[8]
Fe(BCC)	Mn	1063~1173	224.5	0.756	[9]

Diffusion coefficients of Fe, Cr and Mn at 800ºC are therefore: 4.14×10^{-12} cm^{2}s^{-1}, 5.51×10^{-12} cm^{2}s^{-1} and 9.00×10^{-12} cm^{2}s^{-1} respectively. Take the actual sample grain size in this study, which is 0.182mm, and the grain boundary thickness as 10Å [6], and the exposure time is 900s, the quantification criteria are calculated as follows, shown in Table 2.

Table 2 Quantified criteria calculated for experimental condition of the present study

Criteria \ Elements	Cr in Fe (BCC)	Fe in Fe (BCC)	Mn in Fe (BCC)
$(Dt)^{1/2}$	6.788×10^{-5} cm	6.106×10^{-5} cm	9×10^{-5} cm
100δ	1×10^{-5} cm		
$d/20$	9.1×10^{-4} cm		

Therefore, the diffusion kinetic type of the samples in the present study falls into type B regime, $100\delta < (Dt)^{1/2} < d/20$, which is mixed volume diffusion and grain boundary diffusion.

According to the mean diffusion distance criterion, under lower temperature or shorter times, type C diffusion will operate. Diffusion will occur only through grain boundaries without contribution from bulk transport. The $(Dt)^{1/2}$ value is calculated for the conditions of present study and is plotted in Figure 5. For the experimental conditions in this study, it would take only 20 seconds for the diffusion to transit from type C to type B. Although the 40-second heating time from room temperature to 800ºC could prolong the type C regime, type C should still only occur for a very short time comparing to the 900 seconds isothermal exposure at 800ºC. In another word, the type B diffusion is well conformed for the high temperature exposure time of present study. Therefore, it is appropriate to study GB diffusivity with the grain structure shown in Figure 4c.

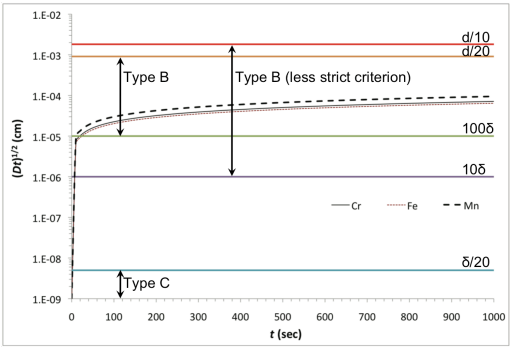

Figure 5 Mean diffusion distance calculated for Cr and Fe in a BCC matrix of iron is plotted versus time in an exposure time of 1000 seconds at 800ºC.

2.2.3 Orientation Imaging

Electron backscattered diffraction (EBSD) was used to generate orientation maps of the polycrystalline alloy surfaces before oxidation on the specimen. The specimen was then mechanically polished and electro-polished prior to EBSD mapping. The EBSD map was collected using an EDAX-TSL Hikari high-speed detector controlled by TSL OIM Data Collection v5.21 software. The backscattered diffraction patterns were collected using an accelerating voltage of 25 kV at 9.8 nA. Orientation data was collected with a resolution of 10 microns. The orientation of the crystal lattice of each grain with respect to an arbitrary reference frame was represented in the form of the three "Euler angles".

2.3.4 EBSD Mapping Data Analysis

The EBSD map was cropped and poorly indexed points were removed using the grain dilation procedure in the TSL OIM analysis software with minimum disorientation angle set as 5º. After clean-up, a single orientation was assigned to each grain. The grain boundaries were reconstructed by fitting line segments between triple points on a hexagonal grid such that the boundary segments did not deviate from the true boundary position by more than two pixels.[10] Next, the disorientation angle between two neighboring grains was calculated for each grain boundary segment with a low angle cut-off of 5º. The TSL OIM Analysis software expressed the ''misorientation'' of two grains in an angle-axis pair convention. The software read the orientation information of the two neighboring grains and returned the rotation angle that has the smallest value of misorientation angle possible. This minimum rotation angle is known as the "disorientation angle". With the TSL analysis software, the CSL boundaries up to sigma 31 were also identified.

2.2.5 High Temperature Exposure

Polished samples were oxidized for 15 minutes at 800ºC in dry air. Steel oxidation in air is generally comprised by an initial, transient stage and a subsequent transition to steady stage.[11,12] During the initial stage, the oxidation is limited by gas phase transfer and/or dissociation, therefore the surface character of the alloy plays a major role in this stage. After the scale layer reaches certain thickness, the diffusion through the oxide layer becomes rate controlling and the kinetics is parabolic, which is called steady stage. To study the relation between alloy grain boundary diffusion and GB charactertistics, the diffusion has to be controlled by the alloy, which means the oxidation must be transient oxidation.

However, the study of transient oxidation requires fast heating and cooling rate. The alloy in the present study was oxidized in a hot-stage attached to a confocal scanning laser microscope (CSLM). The hot-stage is comprised of a gold-image furnace and a halogen lamp as shown in **Figure 6**. The furnace chamber is ellipsoid-shaped so that the radiation from the halogen lamp (located at the lower focus of the ellipsoid) is reflected by the gold furnace wall and concentrated on the sample placed in the crucible (upper focus of the ellipsoid). With this design, the furnace can achieve a high heating rate, for example, heating from room temperature to 800 ºC takes 40 seconds, which is very important for studying transient stage oxidation. A thermocouple is placed near the sample surface to measure the temperature. The measured temperature is used to control the heating intensity, and the temperature profile of the oxidation experiment is always programmed prior to oxidation. To ensure the accurate temperature measurement during heating, the readings of the thermocouple were calibrated by heating pure metals of known melting temperatures.

Before every oxidation experiment, the furnace chamber was evacuated and refilled with dry air, which was subsequently allowed to flow for 5 minutes. This evacuation-and-refilling step was repeated three times. The flow rate of dry air was controlled at 500 ml/s during high temperature exposure. The required heating time from room temperature to 800 °C was 40 seconds and the samples were maintained at this temperature for 15 minutes after which they were cooled to room temperature in another 40 seconds. The oxidized samples were then used for scale characterization.

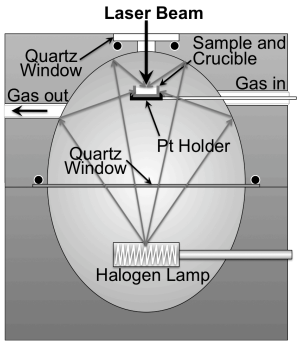

Figure 6 Schematic of the gold-image furnace.

2.2.6 Observation of Scale Ridges

Upon completion of the EBSD mapping, the specimen was subsequently oxidized under the conditions described in section 2.2.5. The scale ridges formed were observed with SEM at an accelerating voltage of 5kV and compared to the GB map obtained before oxidation.

Finally, to establish a reliable relationship between the scale ridge size and misorientation of the alloy grain boundaries, it was necessary to evaluate the changes in alloy GB characteristics after the 15-minute high temperature exposure, as shown in Figure 7.

The scale and scale ridges of a small area of several square microns across two grains were first milled away by focused ion beam (Figure 7a). Then the alloy grains under the scale were exposed and scanned with the OIM system (Figure 7b), and GB disorientations were later calculated from the EBSD maps. This milling-and-EBSD step was repeated for 24 different sites to include a variety of different types of grain boundaries.

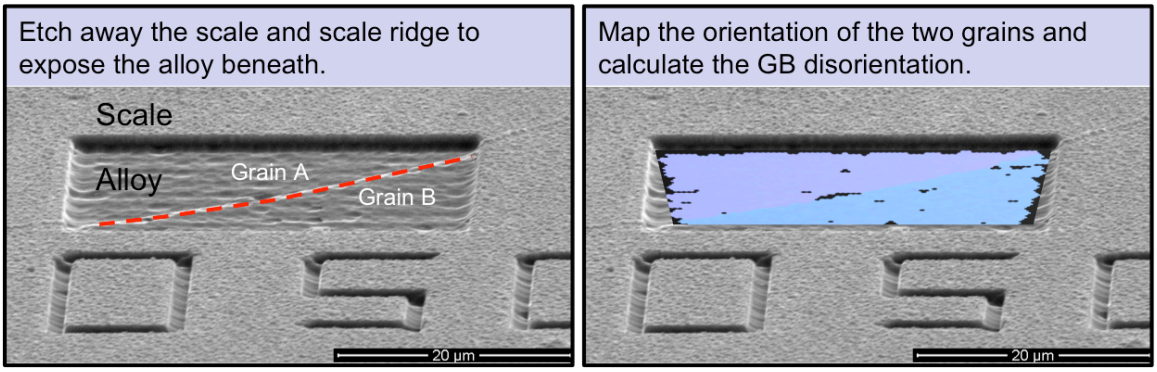

a) **b)**

Figure 7 The milling-and-EBSD of the alloy after oxidation

Comparison of the GB characteristics measured before and after oxidation indicated that the disorientation angles in most of the cases varied within several degrees, which were acceptable system errors: all the low-angle boundaries examined stayed as low-angle boundaries during oxidation; most coincident site lattice (CSL) boundaries (special boundaries) remained as CSL boundaries, and disorientation angles for high-angle boundaries barely changed. Therefore, it was feasible to relate scale ridge morphology obtained with SEM after oxidation to the GB characteristics measured prior to oxidation.

3. Results

To further investigate the relationship between the alloy grain boundary characteristics and the oxide ridges, the alloys were annealed in pure Ar prior to oxidation to be more readily quantified in terms of boundary types and characteristics. Figure 8a shows the EBSD mapping from annealed sample, and corresponding coloring of the grains based upon grain orientation can be found from the inverse pole figure of ferrite (Figure 8b). The alloy grain boundaries were reconstructed from the cleaned up EBSD map, as shown in Figure 8c, in which the green color indicates low disorientation angle (<15º) boundaries, and the black color indicates boundaries with disorientation angles larger than 15 º.

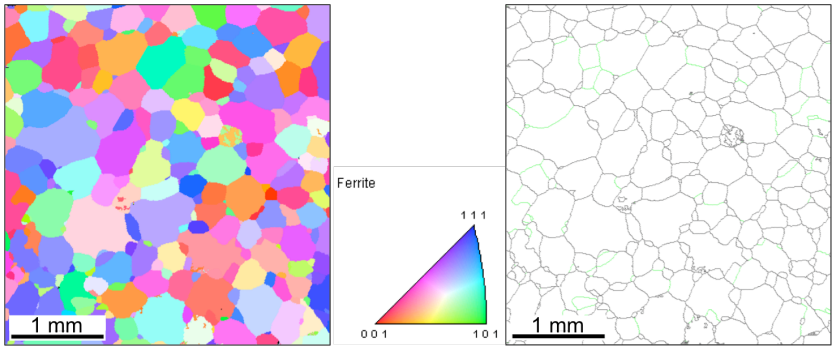

a) b) c)

Figure 8 Original EBSD map was cleaned up with "grain dilation" and then the "single (average) orientation" method. a) EBSD map of the polycrystalline alloy surface after cleaning up. b) The inverse pole figure of ferrite. c) Reconstructed grain boundary map, in which the green color indicates low disorientation angle (<15º) boundaries, and the black color indicates disorientation angle larger than 15º.

Figure. 9a is a plane-view SEM image of several scale ridges, which appear in a brighter contrast in secondary electron images. The two-headed arrow across each segment of ridge indicates the disorientation angle, θ, measured for the alloy GB underneath. Figure 9b shows a grain boundary map and an EBSD map, from top to bottom respectively, of the area where the SEM image was taken. Figure 9c highlights with a square the location on the sample surface where the SEM image was obtained. Comparing Figure 9a with Figure 9b, it is clear that the scale ridges outlined the alloy grains beneath, and matched well with the grain boundary map. Moreover, the GB segment circled in Figure 9b, which corresponds to a low-angle boundary, has a very small ridge (circled in Figure 9a) that has grown on top of it. In fact, almost all the alloy GBs on the sample surface with low disorientation angles (below 15º), in green color, have no or very small ridges on top of them after oxidation. (There are also some outliers: some alloy GB with a disorientation angle larger than 15º have smaller ridges on top of them as well; a few low angle boundaries have ridges comparable in size to high-angle boundaries.)

It was mentioned by Thorning *et al.*[13] that coincident site lattice boundaries were expected to have much lower diffusivities than non-special boundaries with the same disorientation angle. When examining the scale ridges in the current study, small or no ridges were found on all of the Σ3 boundaries, with no exceptions. One example is shown in Figure 10. Very small ridges were also found on a few Σ5 boundary segments and even one Σ11 boundary segment. When the inverse of the fraction of coincident sites exceeds 13, "normal" scale ridge formation was observed, and it seemed that it was the disorientation angle that had the most influence in terms of scale ridge formation. For example, the size of the ridge grown on top of a Σ19 boundary was approximately the same as other ridges formed on the non-sigma boundaries of approximately the same disorientation angle.

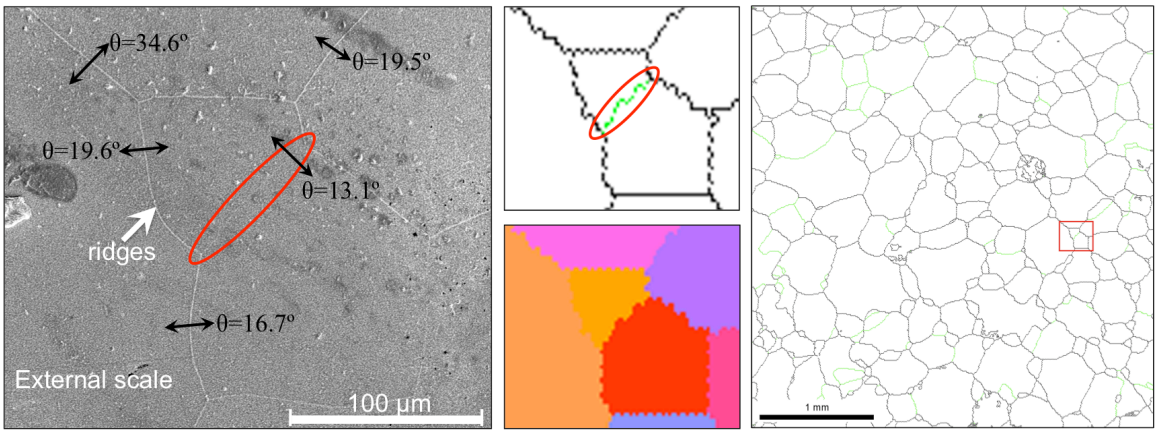

a) b) c)

Figure 9 SEM secondary electron image of the scale ridges in a small area. b) A grain boundary map and an EBSD map, from top to bottom respectively, of the area where the SEM image was taken; the disorientation angle of the circled GB segment is 13.1° c) The location on the sample surface where the SEM image was obtained.

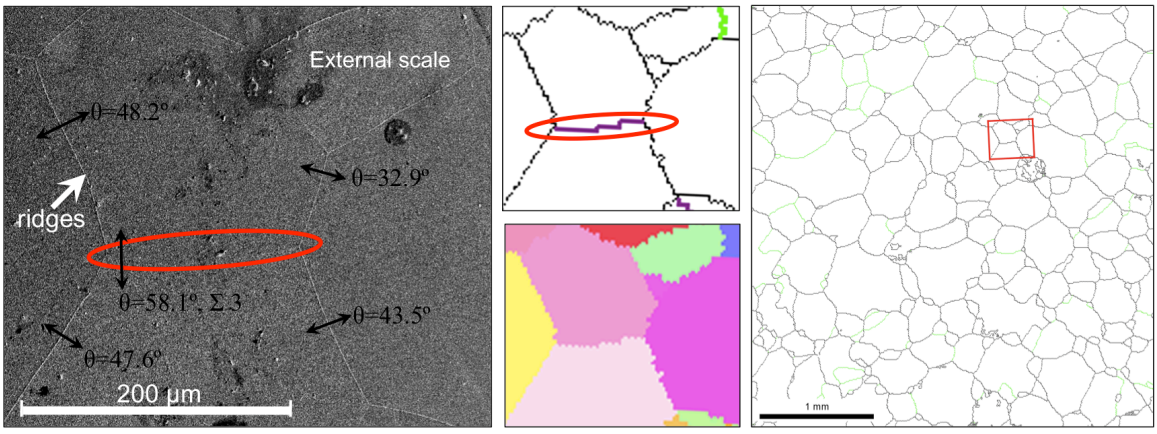

a) b) c)

Figure 10 a) SEM secondary electron image of the scale ridges in a small area. b) A grain boundary map and an EBSD map, from top to bottom respectively, of the area where the SEM image was taken. The circled GB segment is a Σ3 boundary. c) The location on the sample surface where the SEM image was obtained.

Figure 11 is a plot that summarizes the disorientation angles of 385 grain boundary segments of the alloy surface and the sizes of scale ridges that grew from them. The ridges size was graded on a 0-5 scale qualitatively. Size "5" is the largest ridge size found on the oxidized sample surface, and size "0" means no ridge was observable; any size in between "5" and "0" were given 1, 2, 3 or 4 accordingly, from small to large. The sizes were graded with scale ridge micrographs of the same magnification. When all the ridges were given a certain size, the disorientation angle of the alloy GB segment underneath each ridge was calculated using the OIM Data Analysis v5.0 software and was rounded up to the nearest integer value. The ridge sizes corresponding to the same disorientation angle were averaged, and the standard deviation of the ridge size for each disorientation angle was also calculated. The disorientation angles were then plotted against average ridge sizes and the standard deviation was included in the plot as error bars (Figure 11). Note that the negative error bars extended below ridge size "0" were cut, because negative ridge size was never observed, and similarly, the positive error bars extended above ridge size "5" were physically meaningless.

The data plotted in Figure 11 was further binned by 5º, **Figure 12**, which better revealed the relation between the ridge size and GB characteristics. It can be seen from the figures below that the low angle boundaries with disorientations in the range of 6-10º have the smallest ridges grown from them with little scatter in the size. For 10º to 20º, scale ridge sizes increased with increasing disorientation angle. For boundaries larger than 20º, large ridges prevail. Exceptions were observed around 20º and 30º, and the ridge size dropped significantly approaching 60º. In this study, most of the 59º and 60º boundaries are Σ3 boundaries.

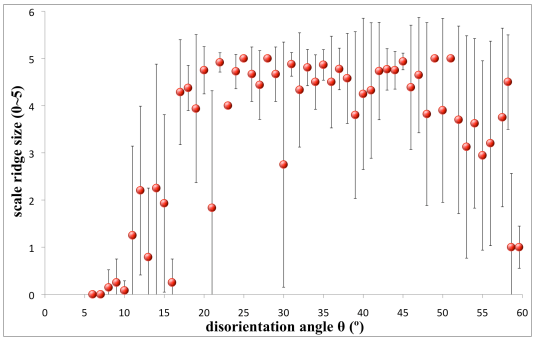

Figure 11 The disorientation angles were plotted against average ridge sizes with the standard deviation included in the plot as error bars.

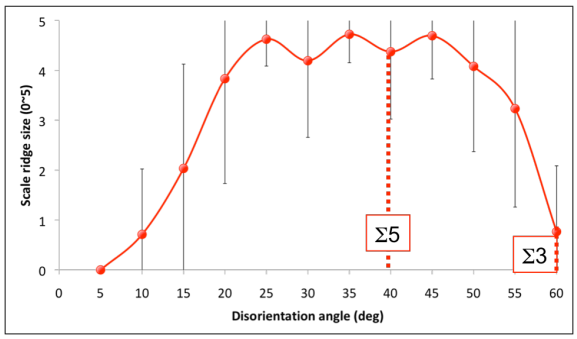

Figure 12 The disorientation angles were plotted against average ridge sizes with a binning resolution of 5º.

4. Discussion

From the results in the current study (Figures 9~12), it appears that not all the grain boundaries intersecting the scale/alloy interface are associated with oxide ridges and there is a variation in the sizes of the ridges. Furthermore, the fact that a correlation between scale ridge sizes and GB characteristics was revealed suggested that GB diffusivity must be dependent upon GB structure and/or characteristics.

Although there have been many experimental investigations that indicate GB diffusivity is dependent on the misorientation between grains, the relation between GB structure and the corresponding diffusivity has only been studied for a limited number of well-defined boundaries.[4,14,6]

The first quantitative study of GB diffusion was carried out by Turnbull and Hoffman in 1954.[14] They found in a tilt grain boundary of silver bicrystals that the δD_b increased with increasing tilt misorientation (θ), following a $\sin(\theta/2)$ variation for small θ. Later work also revealed that GBs with large misorientation angles exhibited cusps on a δD_b vs. θ plot, at angles corresponding to those of sigma boundaries (coincident site lattice misorientation angles).[6] In the present study, similar trends were found as those mentioned in [14] and [6].

Recent studies of grain boundary diffusivity,[15,16,17,18] are significantly scattered in terms of grain boundary diffusion coefficients measured in several of metal and oxide systems. Perhaps the variation of the structures of the GBs studied by these researchers could be one cause of the data scattering, since it was observed in this study that GBs with different characteristics had different diffusivity.

However, few studies were dedicated to relationships between scale ridge formation and grain boundary characteristics. Thorning *et al.*[13] found that intergranular oxidation at high-angle alloy grain boundaries had a pronounced effect on initial oxide morphology on the alloy surface,

whereas no such effect was observed at low-angle grain boundaries in a TRIP steel. They also investigated the scale ridges that were associated with alloy grain boundaries, but no unique correlation between grain boundary disorientation angle and the observed heterogeneities in oxide ridge evolution was found.

The grain boundary misorientation was described in this study as the disorientation and the major types of grain boundaries in our study were low-angle non-special GBs, high-angle non-special GBs and CSL boundaries. A clear relation between scale ridge size and alloy GB disorientation angle was revealed: the scale ridge size increased with increasing disorientation angle as shown in **Figure 11** and **Figure 12**. Moreover, CSL boundaries with low sigma numbers, i.e. Σ3 and Σ5 boundaries, were found to possess low diffusivity. This was indicated in **Figure 11** as a cusp-like drop in scale ridge size at the corresponding angles for Σ3 (60º/[111]) and Σ5 (37º/[100]) boundaries. In Figure 10, a specific example of such a case is shown. It seems reasonable that Σ3 and Σ5 boundaries are associated with better atomic fit at the GB interface which implies a smaller amount of vacancies and/or less complicated dislocation structures would be required within the grain boundaries themselves. Therefore the expected increase in the GB diffusion coefficient with disorientation angle may not be prevalent in these cases.

The effect of grain boundary misorientation on GB diffusivity as shown in **Figure 12** will be discussed here in terms of diffusion coefficient and/or diffusivity. Grain boundary diffusivity at a given temperature *T*, the product δD_{GB}, is composed of a pre-exponential factor, D_{oGB}, (assumed to be independent of pressure and temperature) and an exponential term including activation energy and temperature, which is similar to the diffusion coefficient of volume diffusion. The grain boundary thickness is δ and D_{GB} the grain boundary diffusion coefficient.

D_o for volume diffusion is more or less constant at a given temperature,[19] from which it can be deduced that D_{oGB}, similar to D_o, can be taken as constant for a solid of a given structure and bond type,[19] assuming the same vacancy diffusion mechanism operates for both volume diffusion and GB diffusion. In other words, the structure of the grain boundary, i.e. misorientation, has little influence on D_{oGB}.

On the other hand, the exponential term in D_{GB} could have a strong dependence to disorientation angle and grain boundary structure. Differences in free space at different boundary interfaces should result in a difference in diffusion activation energy and activation volume. The free space at a small-angle boundary can be expected to be smaller than that of a large-angle boundary, and particularly for some Σ3 boundaries, the free space at the boundary should also be very small. Therefore, although the volume of a boundary vacancy formation is the same for small-angle or CSL boundary as that for a large-angle non-special boundary, when a diffusive jump occurs in a small-angle or CSL boundary, the free volume that is associated permanently with the boundary will make the jump possible with more local dilation than that required within a high-angle non-special boundary plane; therefore the volume needed for the migration of a boundary vacancy, as well, should be larger than that of a vacancy at high-angle non-special boundary. This would result in higher activation energy and activation volume that give rise to a decrease of the GB diffusion coefficient.

The GB free space is also associated with grain boundary thickness δ, although the effect is not as prominent as the exponential terms: activation energy and volume. The δ of a small-angle boundary (5~10º) is smaller than that of boundaries larger than 20º. It is also noticeable that for boundaries above 20º, the scale ridge size does not vary that much, unless special (CSL)

boundaries are present. This is in accordance with the fact that boundary thickness and the degree of disorder at the GB interface are not so different for non-special boundaries larger than 20º [4] and therefore does not influence diffusivity much. However, low sigma number CSL boundaries, despite their large disorientation angles, e.g. 60º for Σ3 boundary, have much less disordered boundary interfaces than non-special boundaries with the same disorientation angle. The boundary thickness of CSL boundaries is therefore expected to be much smaller than that of the non-special boundaries. The lower sigma number boundaries share more sites between adjacent grains, therefore the minimum grain boundary width required would decrease as more lattice sites are shared between neighboring grains.

However, one should notice that the alloy surface composition after oxidation is different from point to point. This probably occurs during high temperature exposure when scale-forming elements diffuse outward from the metal matrix. The variation in surface composition may change the interfacial energy in the alloy grain boundary. As it is known that this change in interfacial energy is unlikely to cause change in grain orientation, it may, however, cause segregation of impurity elements in the grain boundaries, especially in high energy boundaries, which has a fairly strong impact on the diffusivity in those boundaries. However, differentiating such effect on GB diffusivity from the effect of disorientation is not trivial. Since no attempt of measuring GB segregation has been made in this study, the possible effect from impurity segregation on GB diffusivity deserves further investigation.

This investigation of the correlation between scale ridge size and alloy GB disorientation is generally qualitative in nature and phenomenological to some extent. However, by taking a closer look at the abnormal behavior of some GBs, i.e. large-angle non-special boundaries having small ridges over them, several possibilities may be suggested that lead to the anomalous behavior of some grain boundaries.

1. The grain boundary plane may be one cause of anomalous behavior, which was not considered in this study. It has been reported that GB plane has significant influence on the GB properties, such as GB energy, for example for systems in which twin boundaries are present.[24] It was also mentioned that GB plane can influence the GB diffusion.[14] Therefore, if GB plane is considered, a more precise relation between GB diffusivity and GB characteristics could be expected.

2. GB connectivity in the GB network might be another reason for the anomalous behavior of some grain boundaries. By far, our investigation concerned only the first layer of alloy grains next to the oxidizing atmosphere. If a low diffusivity GB is connected to a high diffusivity boundary that intersects the free surface, the supply of scale-forming elements might be cut off or at least significantly reduced that would yield small ridge.

3. If a considerable amount of intergranular oxides, illustrated in Figure 15, formed along grain boundaries, then after a while diffusion would have no longer been solely under the effect of the misorientation of the alloy grain boundaries but also the diffusion through the internally formed oxides or along the internal oxide/alloy interface. Therefore, the extent and nature of the intergranular oxides formed along GBs must also be taken into account with relevant data available.

5. Conclusions

Scale ridge growth on the surface of alloys similar to Crofer 22 stainless steel was studied.

SEM imaging of the scale ridges combined with EBSD mapping of underlying alloy grains

revealed a relation between ridge size and the misorientation of the alloy GB underneath. Among non-special grain boundaries, small ridges usually corresponded to small angle boundaries beneath, and large ridge corresponded to large angle boundaries. Sigma 3 and 5 boundaries also had very small ridges on top of them, despite their large disorientation angles.

If GB diffusivity can be represented by scale ridge size, then the GB diffusivity is small when activation energy and/or activation volume is large, which is the case of a less disordered GB interface: either a small angle boundary or a CSL boundary.

6. Future work

The following work is planned as the improvement to the current investigation.

1) Quantifying the size of ridges by atomic force microscopy (AFM) as the example shown in Figure 14;

2) Determining the grain boundary plane by obtaining at least one more slice of orientation map on the surface;

3) Experimental measurement of intergranular oxides and/or segregation of impurities at grain boundaries.

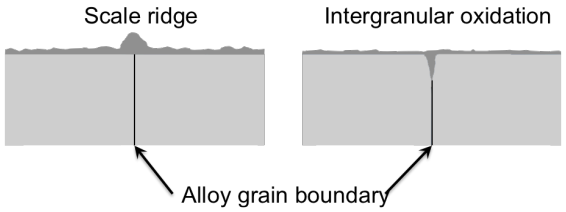

Figure 13 Schematic of scale ridge and intergranular oxidation.

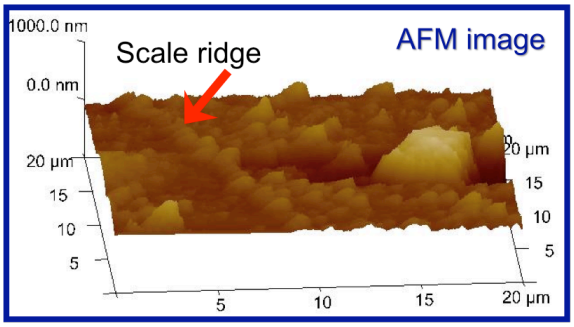

Figure 14 AFM measurement of a scale ridge.

References

[1] N. Bricks, G. H. Meier and F. S. Pettit, High-temperature Oxidation of Metals 2nd Ed., Cambridge university press, Cambridge, UK, (2006).
[2] W. J. Quadakkers, J. Piron-Abellan, V. Shemet and L. Singheiser, Mater. High Temp., 20(2), 115 (2003).
[3] L. M. Fernandez Diaz, J. Zhu, G. R. Holcomb, P. D. Jablonski, D. E. Alman, S. Sridhar, Defect and Diffusion Forum, 283-286, 425 (2009).
[4] A. P. Sutton and R. W. Balluffi, Interfaces in Crystalline Materials, Oxford University Press, Oxford, (1995).
[5] L. G. Harrison, Trans. Faraday Soc., 57, 1191 (1961).
[6] I. Kaur, Y. Mishin and W. Gust, Fundamentals of Grain and Interphase Boundary Diffusion, 3rd Ed., John Wiley & Sons Ltd., New York (1995).
[7] H. Oikawa. Tech. Rep., Tohoku Univ., vol. 46, 1982, 67-77.
[8] A.M. Huntz, M. Aucouturier et P. Lacombe. Compt. Rend. Acad. Sci., C265, 1947, 554-

557.
[9] K. Nohara and K. Hirano; "Proc. Intern. Conf. on Sci. and Tech. of Iron and Steels", Suppl. to Trans. Iron Steel Inst. Japan., 1971, 1267-73.
[10] Wright SI and Larsen RJ, J. Microsc., 205, 245 (2002)
[11] D.P. Whittle and J. Stringer, Improvements in high temperature oxidation resistance by additions of reactive elements or oxide dispersions. Philosophical Transactions of the Royal Society of London, Series A, Vol.295, No.1413, p. 309-329 (1980)
[12] O. Kubaschewski, and B. E. Hopkins, Oxidation of Metal and Alloys. Academic Press, London, (1962).
[13] C. Thorning and S. Sridhar, Philos. Mag., 87(23), 3479 (2007).
[14] D. Turnbull, R. E. Hoffman, Acta Metall., 2(3), 419 (1954)
[15] W. Preis and W. Sitte, Solid State Ionics, 79, 765 (2008).
[16] J. S. Dohie, J. R. Cahoon and W. F. Caley, J. Phase Equilib. Diffus., 28(4), 322 (2007)
[17] T. Nakagawa, I. Sakaguchi, N. Shibata, K. Matsunaga, T. Mizoguchi, T.Yamamoto, H. Haneda, and Y. Ikuhara, Acta Mater., 55, 6627 (2007).
[18] A. Inoue, H. Nitta and Y. Iijima, Acta Mater., 55, 5910 (2007).
[19] A. M. Brown and M. F. Ashby, Acta Metall., 28, 1085 (1980).